Pressure Line Broadening and Feasibility of CO_2 Profile Retrieval using Near Infrared Observations of an Absorption Line

Run-Lie Shia[1], Le Kuai[2], Michael R. Line[1], John T. Trauger[2] and Yuk L.Yung[1]

[1] Division of Geological and Planetary Sciences, California Institute of Technology, 1200 East California Blvd., Pasadena, CA 91125

[2] Jet Propulsion Laboratory, California Institute of Technology, 4800 Oak Grove Drive, Pasadena, CA 91109

To be submitted to *Appl. Opt.*, January, 2013

Abstract

Analytic expressions are derived for the transmittance and reflectance of sunlight and their Jacobians for an absorption line with Lorentz line broadening. Rodgers information analysis is applied to calculate the information content, the degrees of freedom and the averaging kernel for a simple atmospheric model to investigate the feasibility of retrieving the profile of CO_2 using near-infrared (NIR) measurements over a single absorption line. The results have implications for the design of future space instruments with high spectral resolution and high signal to noise ratios to obtain global scale information on the CO_2 vertical distribution which is important for inferring the sources, sinks, and transport of CO_2.

1. Introduction

CO_2 is the most important anthropogenic greenhouse gas. Its increase in the atmosphere is the main cause of the rise in the globally averaged surface temperature [1]. The prediction for climate change by the end of this century is dire if the trend of increasing CO_2 content is not contained. To quantitatively determine the global sources and sinks of CO_2, satellite remote sensing is a powerful tool. Current measurements of reflected solar NIR radiation from space, e.g. GOSAT, [2-4], and the future OCO-2 mission [5], are and will be used to retrieve the column averaged CO_2 mixing ratio, X_{CO2}. Measurements of solar NIR transmittance are also obtained at surface stations (TCCON, [6,7]). Although the global distributions of X_{CO2} are quite useful for constraining CO_2 sources and sinks, the vertical distribution of CO_2, especially in the lower and the middle troposphere, is needed for understanding the hemispheric transport of CO_2 and the carbon cycle [8, 9].

In this study we use a simple atmospheric model to demonstrate the feasibility of retrieving multiple pieces of CO_2 vertical profile information from high signal to noise ratio (S/N) and high spectral resolution atmospheric spectra. In the model only one CO_2 line in the NIR region is selected and it is assumed to have Lorentz line broadening only, so the transmittance at the surface and the reflectance at the top of the atmosphere (TOA) of the incident sunlight can be derived analytically, along with their derivatives, Jacobians. The transmittance, reflectance and the Jacobians of these quantities, derived in Appendix A, are used to calculate the information content (H), the degrees of freedom (d_s) and the averaging kernel matrix (A) using formulas in [10]. For high S/N and high spectral resolutions, the calculated H, d_s and A show that measurements over one line could provide sufficient information for the CO_2 vertical distribution to be retrieved. These accurate calculations provide critical insights into the physics of using those spectra for CO_2 vertical retrievals. A more comprehensive evaluation of vertical profile retrievals using satellite observations is under way.

This paper is divided into five sections. A brief discussion of Rodgers information analysis is presented in section 2. The information content, the degrees of freedom, and the averaging kernel matrix over a NIR CO_2 line with pressure-independent line broadening and with the pressure-dependent Lorentz line broadening are calculated for different S/N and different spectral resolutions in section 3 to demonstrate the feasibility of CO_2 profile retrieval. In section 4, Jacobians over the same line from the retrieval models of TCCON and GOSAT are compared to those of the analytical solutions in section 3. Implications of this study for a profile retrieval are discussed in section 5.

2. Rodgers information analysis

In optimal estimation theory, the degrees of freedom measures the number of independent variables that can be retrieved and the Shannon information content is the total amount of information (in bits) gained from the measurements [10]. In Appendix A the analytic formulas for the transmittance at the surface, reflectance at the TOA and their Jacobians K are derived for a CO_2 line with Lorentz broadening. The normalized Jacobian matrix ($\tilde{K}$) is calculated from K, the measurement error covariance (S_ε) and the a priori covariance matrix (S_a) using the following equation

$$\tilde{K} = S_\varepsilon^{-1/2} K S_a^{1/2} \tag{1}$$

H and d_s are defined by

$$H = \frac{1}{2}\sum_i \ln(1+\lambda_i^2) \tag{2}$$

$$d_s = \sum_i \lambda_i^2 / (1+\lambda_i^2) \tag{3}$$

where λ_i are the singular values of $\tilde{K}$ [10]. In the cases studied in the following section, a diagonal a priori covariance matrix for CO_2 with error of 3% is used. Another useful variable is the averaging kernel, which is defined as [10]

$$A = GK \tag{4}$$

where G is the gain matrix,

$$G = S_a K^T (K S_a K^T + S_\varepsilon)^{-1} \tag{5}$$

The averaging kernel is a square matrix. Its column and row vectors have the same dimension as the state vector, which in our atmospheric model is the CO_2 concentration in every pressure grid box. It is the ratio of the change in the retrieved state vector to the change in the true state vector. If there is no correlation between the components of the state vector, the measurements are accurate, and the model has all the physical processes simulated well, then the averaging kernel approaches the unit matrix. That is, for any change in a component of the true state vector the corresponding component of the retrieved state vector changes by the same amount and all other components of the retrieved state vector are unchanged.

3. H , d_s and A in the transmittance and reflectance of NIR solar radiance

We demonstrate our idea with numerical calculations using a CO_2 line at 6243.9 cm^{-1}; the instrument resolution is 0.02 cm^{-1}. The line strength is S =1.53×10^{-23} cm and the Lorentz line broadening constant A=7.2×10^{-5} cm^{-1} mb^{-1} ([11] and references therein). The model atmosphere is evenly divided into 100 layers in pressure from the surface, P_s = 1000 mb, to the top of the atmosphere, P_t = 0 mb.

We have tested the following four cases:

Case A. Transmittance at the surface with pressure-independent line broadening, assuming the absorption cross section of CO_2 at all pressure levels has the Lorentz line broadening at $\frac{1}{3}P_s$, using the 30 channels and $\Delta\nu = 0.02$ cm^{-1};

Case B. Transmittance at the surface with Lorentz line broadening, using the 30 channels and $\Delta\nu = 0.02$ cm^{-1};

Case C. Transmittance at the surface with Lorentz line broadening, using the 150 channels and $\Delta\nu = 0.004$ cm^{-1};

Case D. Reflectance at the top of the atmosphere with Lorentz line broadening using 30 channels, and $\Delta\nu = 0.02$ cm^{-1}.

In all cases, the spectral range of the channels covers 8 times the line width at the surface (0.072 cm^{-1}). The solar zenith angle θ is set to be zero, *i.e.* $\mu_0 = \cos\theta = 1$ and the viewing zenith angle of reflection in case D is also equal to zero, so $\mu = 1$. H , d_s and A could change with changing zenith angle. In case D we select the surface reflectivity $\rho = 1$. For $\rho < 1$, H and d_s would be less. We will discuss these effects in a follow-up paper.

H , d_s , and A for these cases are calculated using the formulas in Appendix A and Eqns. (4) and (5). They are plotted in Fig. 1, the first column (Figs. 1a, 1d, 1g, and 1j) is the transmittance/reflectance for the four cases, respectively, the second column (Figs. 1b, 1e, 1h, and 1k) is the Jacobian for each case, and the third column (Figs. 1c, 1f, 1i, and 1l) is for the column vectors of A multiplied by 100. The colored dots on the transmittance/reflectance curves in the first column indicate the spectral channels. For case C, which has 150 channels, only 1 in 5 channels is selected for plotting (the total number of dots remains 30, instead of 150) for esthetic purposes. The colors of the Jacobian in the second column match the colors of the dots of the corresponding channels on the transmittance/reflectance curves in the first column. The total number of the colored curves of A in the third column is 100, which is the dimension of the state vector of CO_2. The black line in each panel of the third column of Fig. 1 is the sum of all column vectors of A. For the ideal case mentioned before, the averaging kernel is a unit matrix and this would be a straight vertical line at 1.

For case A, which has pressure-independent line broadening, the Jacobians and the column vectors of A are vertical lines (Fig. 1b and 1c). This means the transmittances contain no information on the vertical distribution of CO_2. Adding CO_2 at different altitudes would have the same effect on the transmittance at the surface. The only variable that affects the transmittances in this case is the total amount of CO_2. This means d_s is always less than or equal to 1. From the point of view of numerical calculations, this is because all of the columns of the Jacobian matrix, K are linearly dependent so that the scaled Jacobian $\tilde{K}$ has only one nonzero eigenvalue, no matter how large the S/N is, what the a priori is or how large the dimension of the state vector is. Eqn. (4) would only generate $d_s \leq 1$. The H and d_s for different S/N for this case are listed in

Table 1. It shows that higher S/N can increase the information content significantly, but cannot make d_s greater than 1.

Table 1. H and d_s of the transmittance of the solar NIR radiance at the surface vs. S/N for the constant line broadening atmosphere (case A). The S/N for the baseline is 1000 and the spectral resolution 0.02 (cm^{-1})

S/N (×1000)	0.5	1.	2.	10.	100.
H	0.763	1.55	2.48	4.78	8.10
d_s	0.653	0.883	0.968	1.00	1.00

Although the transmittances in cases with pressure-independent line broadening (case A) and with Lorentz line broadening (case B) are similar (Fig. 1a and 1d), their Jacobians and the column vectors of A are quite different (Fig. 1b and 1c vs. 1e and 1f). In case B, the plot shows that the Jacobian and the column vectors of A for each channel is not a vertical line and there is vertical information in the transmittances because the location of CO_2 does make a difference to the measurements of the transmittance at the surface. Now $\tilde{K}$ has more than one non-zero singular value. Accordingly, d_s becomes larger than 1 for large S/N and H also increases (Table 2).

Table 2. Same as Table 1, but with Lorentz line broadening.

S/N (×1000)	0.5	1.	2.	10.	100.
H	0.810	1.90	3.62	9.83	23.1
d_s	0.794	1.40	2.02	3.27	4.69

With finer spectral resolutions, more distinct channels can be measured over one line. This would increase the information content and the degrees of freedom in retrievals. A new case (case C), with 5 times finer spectral resolution than the previous cases (30 channels) is tested with the same line broadening. The transmittances of the two cases with the different spectral resolutions and the same line broadening (Fig. 1d and 1g) are similar, except the minimum of the transmittances for the case with the finer spectral resolution is smaller because the corresponding channel is closer to the line center. In all the cases in this paper the line center is intentionally not

measured, because at the center other line-broadening processes would play a more important role than the Lorentz line broadening in the upper atmosphere. The Jacobians in Fig. 1h are similar to those in Fig. 1e, because only 1 in 5 channels are selected to plot in Fig. 1h. The averaging kernels of two cases are quite different (Fig. 1f and 1i). Comparing Tables 2 and 3, we see that increasing the spectral resolution significantly increases the information content and the degrees of freedom.

Table 3. Same as Table 2, but with spectral resolution = 0.004 cm^{-1}

S/N (×1000)	0.5	1.	2.	10.	100.
H	2.23	4.27	7.16	17.0	37.6
d_s	1.63	2.47	3.32	5.09	7.24

Although the reflected NIR solar radiance at the TOA measured from space-borne instruments is smaller than the radiance measured at the surface (Fig. 1d and 1j), there is still significant vertical information contained in the measurements of reflectance at the TOA because the light goes through the atmosphere twice. The Jacobians for the transmittance and reflectance seem comparable for most channels (Fig. 1e and 1k) owing to the double role that CO_2 plays, once in the incident path and once in the reflected path. Also, the vertical information in the reflectance (case D) (Fig. 1k and 1l) is more evenly distributed than in the transmittance (case B) (Fig. 1e and 1f), which contains more information in the upper atmosphere. The results of the numerical calculations of the reflectance case are listed the Table 4 for different S/N. They are comparable to the transmittance case (Table 2).

Table 4. H and d_s of the reflectance at TOA vs. S/N for the Lorentz line broadening atmosphere. The S/N for the baseline is 1000 and the spectral resolution is 0.02 cm^{-1}.

S/N (×1000)	0.5	1.	2.	10.	100.
H	0.978	2.07	3.70	9.87	23.6
d_s	0.845	1.35	1.94	3.34	4.86

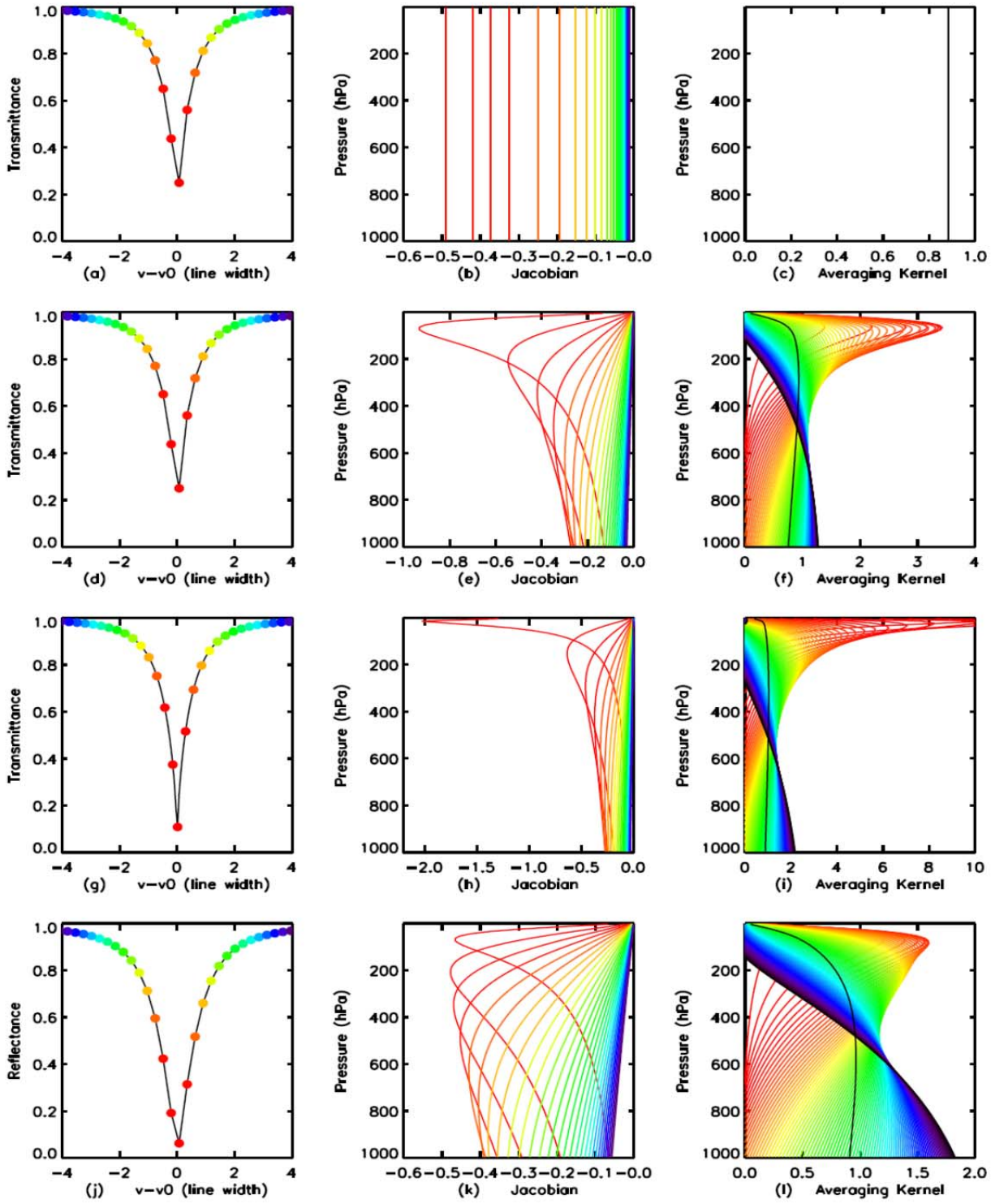

Figure. 1 (a), (b) and (c), Transmittance at the surface, its Jacobian and averaging kernel, respectively, for the case with pressure-independent line broadening for 30 channels; (d), (e) and (f), Same as (a), (b) and (c) but for the case with Lorentz broadening; (g), (h) and (i), Same as (d), (e) and (f), but with 150 channels; (j), (k) and (l), Same as (d), (e) and (f), for reflectance at the top of the atmosphere.

For cases B and D more calculations of H and d_s have been done for different S/N and different spectral resolutions. For every spectral resolution the total number of channels changes accordingly so they still cover 8 times the line width at the surface as in the original cases B and D. The color contour plots in Fig. 2 show how H and d_s vary with the resolving power $R = \nu_0 / \Delta\nu$, and S/N for the transmittance case. Both the resolving power and S/N are quite effective in increasing H and d_s. The color contour plots in Fig. 3 show how H and d_s vary with the spectral resolution and S/N for the reflectance case. It is quite similar to the transmittance case (Fig. 2).

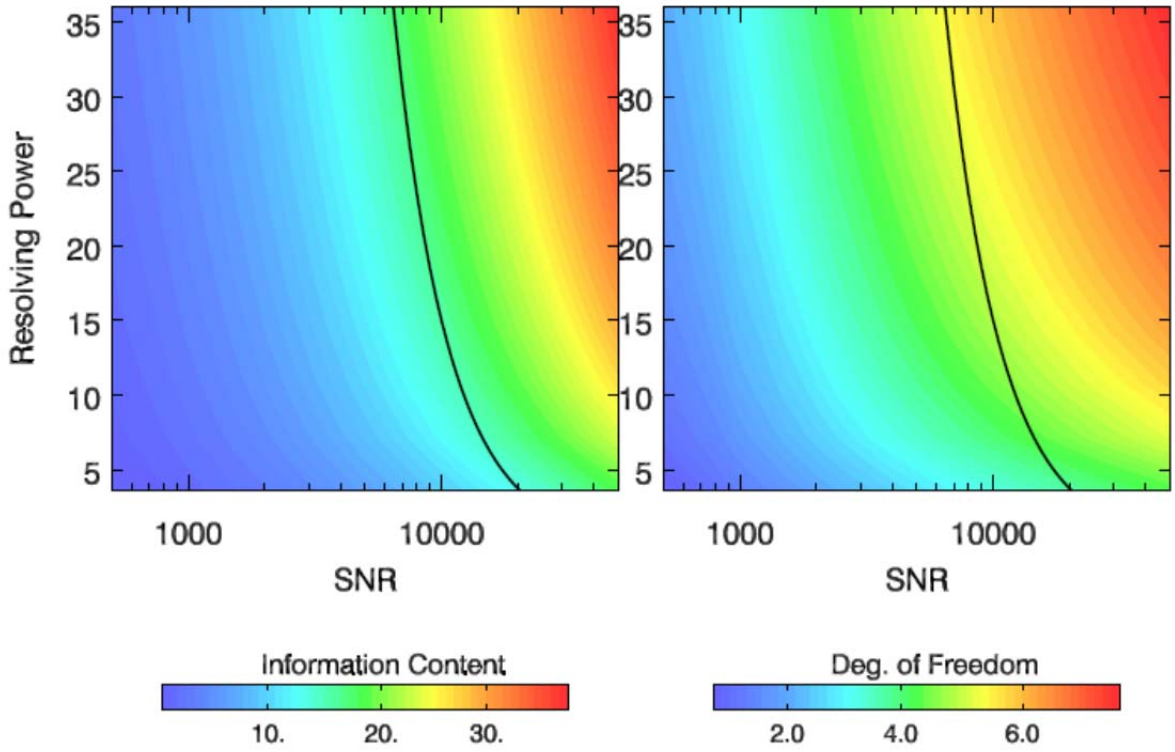

Figure 2. Information content (left) and degrees of freedom (right) contoured as functions of S/N and the resolving power for the transmittance at the surface. The unit for the resolving power is (ν_0 / α_s) =8.67×10^4. The black line shows when the resolution of an instrument changes how its S/N would change correspondingly.

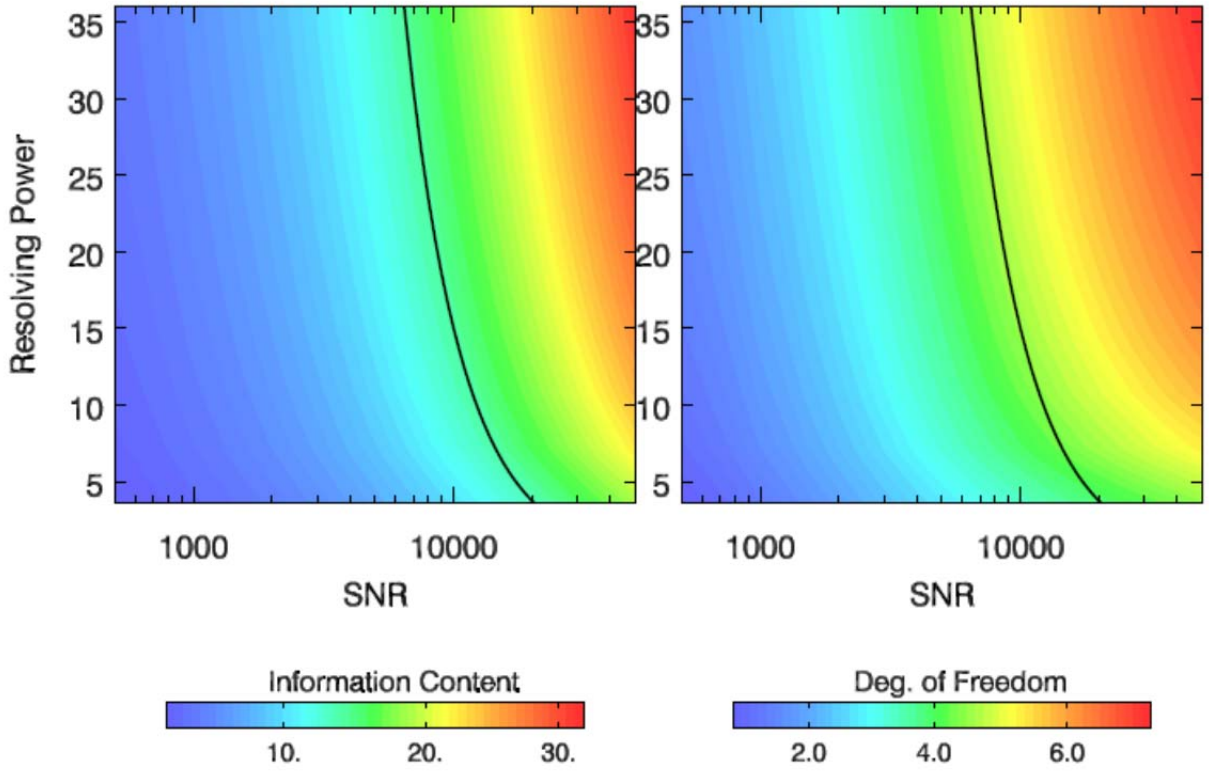

Figure 3. Information content (left) and degrees of freedom (right) contoured as functions of S/N and the resolving power for the reflectance. The unit for the resolving power is (ν_0 / α_s)=8.67×10^4. The black line shows when the resolution of an instrument changes how its S/N would change correspondingly.

For the case that the dominant noise of an instrument is background limited, due to fluctuations in the number of arriving photons, the S/N is reduced when resolving power increases, because fewer photons are received in each channel. The S/N drops as $\sim \sqrt{\Delta\nu} \sim 1/\sqrt{R}$. The black lines in Figs. 2 and 3 show this relation. In this case increasing the resolving power in an instrument would not result in much gain in H and d_s.

4. Transmittance/Reflectance and Jacobians collected from TCCON and GOSAT retrieval models

In the test cases with pressure dependent line broadening in section 3, the CO_2 absorption line has only the Lorentz broadening. In the atmosphere there are other physical processes which

change the CO_2 line profile, *e.g.* the Doppler line broadening. Also, overlapping of lines and the continuum become significant in the wings of a line. As a comparison, the transmittances at the surface and their Jacobian for the same spectral line are obtained from the TCCON/GFIT [12] and GOSAT [13, 14] retrieval models, respectively. The results are plotted in Fig. 4. The Jacobians of TCCON plotted in Fig. 4c are similar to Jacobians of the analytic solutions plotted in Fig. 1e. It seems other line broadening mechanisms in the TCCON case only make the channels near the line center not as effective as in the case with pure Lorentz line broadening in retrieving the CO_2 in the upper atmosphere. Although, some of the Jacobians of GOSAT plotted in Fig. 4d are similar to their corresponding ones in Fig. 4d, it is quite obvious that GOSAT is not as good as TCCON for profile retrieving of CO_2, due to its coarser spectral resolution.

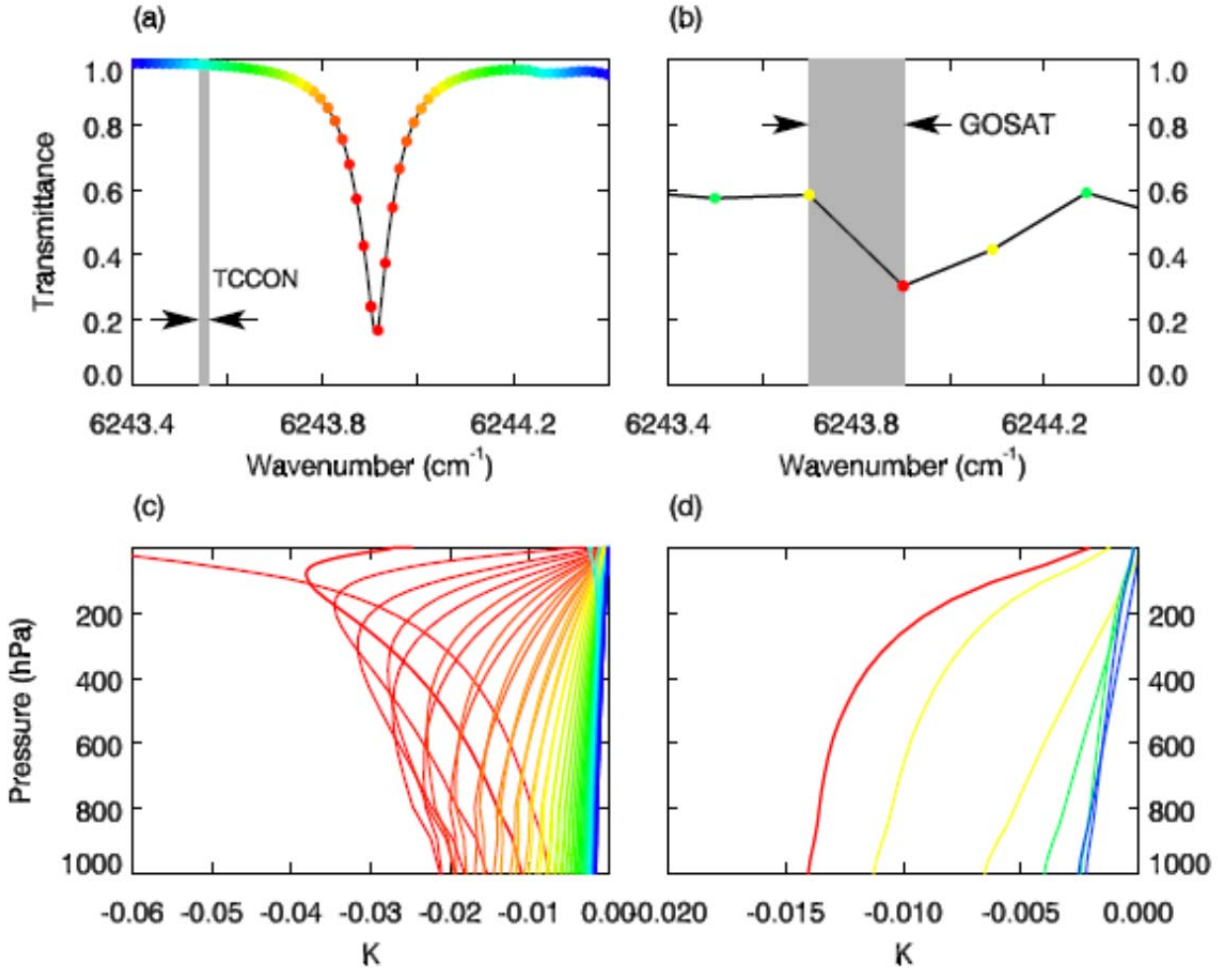

Figure 4. Computed transmittance of the CO_2 line at ν_0 = 6243.9 cm^{-1} viewed at μ_0 = 1.0, (a) and Jacobian, (c), using TCCON forward model. In the CO_2 profile, the blue denotes absorption in the wings, while red denotes

absorption near the center of the line. The spectral resolution of the instrument is indicated by a vertical grey line. (b) and (d) Same as (a) and (c), but for the GOSAT with $\mu_0 = \mu = 1$ and surface reflectivity $\rho = 0.64$.

The vertical coordinate of the TCCON retrieval model is the altitude. The Jacobians obtained from the model have to be scaled by the air mass factor in each grid boxes before they can be plotted in Fig. 4c for comparison with the Jacobians of analytic solution. Otherwise, the peaks of the Jacobians are all located near the bottom of the atmosphere because there is less CO_2 in upper grid boxes, making it difficult to see where the vertical information can be retrieval form observations. Thus, the pressure coordinate, which is used in GOSAT retrieval model seems a better choice.

Kuai *et al.* [15] calculated H and d_s for the TCCON resolution of 0.014 cm^{-1} and S/N = 1000 for the TCCON spectrum and found H =6.80 and d_s =2.72. These values are higher than the corresponding numbers for the simplified line case in Table 2 (the baseline case with S/N = 1000) because many more lines are included in the TCCON retrieval. There is enough information in TCCON to constrain the vertical distribution of CO_2 in the atmosphere. Kuai *et al.* [15] were able to retrieve three partial column CO_2 densities. All three partial columns have roughly the same amount of air mass.

5. Discussion

The measurements of the NIR solar radiation can provide information on the CO_2 vertical distribution through line broadening. Although TCCON observations can be used to retrieve 2-3 CO_2 partial column densities, the measurements of current and near future satellite remote sensing instruments like GOSAT and OCO-2 do not contain sufficient information on the vertical distribution of CO_2, due to their lower S/N and coarser spectral resolution as compared to TCCON.

However, since instruments like those used in GOSAT and OCO-2 can be improved to provide information on the vertical distribution of CO_2 by improving S/N and/or using finer spectral resolution, the possibility of using new instruments, which cover a few CO_2 lines with

much higher S/N and spectral resolution should be considered. Tables 2 and 3 have shown that it is feasible to use measurements from those proposed new instruments to retrieve the profile of CO_2 in the atmosphere. If the new instruments can have 10 times the S/N and 5 times the spectral resolution of TCCON, their measurements would provide enough information (H =17) for more than 5 degrees of freedom for profile retrievals of CO_2.

Using observations over a few spectral lines for profile retrieval has been proposed to retrieve CO_2 and other species in the atmosphere [16-17]. An example of a possible type of instrument is the versatile PEPSIOS, originally designed and built for the study of trace constituents (HD, O_2, CO) in planetary spectra at visible and NIR wavelengths from ground-based telescopes [18]. It is well suited for the measurement of line profiles at spectral resolutions of 0.010 – 0.014 cm^{-1}, similar to the resolution of TCCON in Fig. 4a, with high throughput and improved suppression of the spectral wings. It is a relatively compact instrument, and can be configured for remote sensing from satellites with the spectral resolution and S/N ratio required to allow for profile retrievals of CO_2.

Acknowledgements. We thank Dr. J. Margolis for his valuable suggestions on the noise-resolution relation for instruments, Dr. V. Natraj for helpful comments and GOSAT retrieval data and Dr. S. Newman for her suggestions to improve the manuscript. This research is supported in part by the Orbiting Carbon Observatory 2 (OCO-2) project, a NASA Earth System Science Pathfinder (ESSP) mission and Project JPL.1382974 to the California Institute of Technology.

Appendix A: Transmittance and Reflectance Derivations

1. At the surface

Assuming that Doppler line broadening is negligible, the absorption coefficient of a Lorentz line can be expressed as

$$k_\nu = S \cdot f(\nu - \nu_0) = S \cdot \frac{\alpha}{\pi} \frac{1}{\alpha^2 + (\nu - \nu_0)^2} \tag{1}$$

where S is the line strength, ν is the frequency of the NIR line and the line broadening at pressure P is $\alpha = A \cdot P$, $A = \alpha_s / P_s$, P_s is the surface pressure. For the zenith angle $\theta = 0$, the total optical depth of the atmosphere, τ_ν can be calculated as the integral of

$$d\tau_\nu = k_\nu \cdot n \cdot dz ,$$

$$\tau_\nu = \int_0^\infty k_\nu \cdot n \cdot dz = \int_0^{P_s} k_\nu \cdot \chi \cdot \frac{dp}{mg}, \tag{2}$$

where z is the altitude, n is the number density of, *e.g.* CO_2, χ is the mixing ratio of CO_2, m is the mean molecule mass of the atmosphere and g is the gravitational constant.

Using (1),

$$\tau_\nu = \frac{S\chi}{\pi mg} \int_0^{P_s} \frac{\alpha}{\alpha^2 + (\nu - \nu_0)^2} dp = \frac{S\chi}{\pi mg} \int_0^{P_s} \frac{Ap}{(Ap)^2 + (\nu - \nu_0)^2} dp$$

$$= \frac{S\chi}{2\pi mgA} \int_0^{P_s} \frac{1}{p^2 + [(\nu - \nu_0)/A]^2} dp^2 = \frac{S\chi}{2\pi mgA} \ln \frac{P_s^2 + [(\nu - \nu_0)/A]^2}{[(\nu - \nu_0)/A]^2}$$

$$= r \cdot \ln \frac{P_s^2 + [(\nu - \nu_0)/A]^2}{[(\nu - \nu_0)/A]^2} = r \cdot \ln \frac{\alpha_s^2 + (\nu - \nu_0)^2}{(\nu - \nu_0)^2} \tag{3}$$

where $r \equiv \frac{S\chi}{2\pi mgA} = \frac{S\chi P_s}{2\pi mg\alpha_s} = \frac{SN}{2\pi\alpha_s}$ and N is the CO_2 number density at the surface.

The transmittance at the surface, which is like the measurements of TCCON, is

$$T_\nu = e^{-\tau_\nu} = \left[\frac{(\nu - \nu_0)^2}{\alpha_s^2 + (\nu - \nu_0)^2} \right]^r \tag{4}$$

The calculations of H and d_s use only the finite difference of Jacobians. In the finite difference form,

$$\tau_\nu = \sum_i \Delta\tau_{\nu,i} = \frac{S\chi}{\pi mg} \sum_i \frac{Ap_i}{(Ap_i)^2 + (\nu - \nu_0)^2} \Delta p_i = 2A \cdot r \sum_i \frac{\alpha_i}{\alpha_i^2 + (\nu - \nu_0)^2} \Delta p_i \tag{5}$$

where Δp_i is the size of the grid box in the pressure coordinate.

The transmittance

$$T_\nu = e^{-\sum_i \Delta\tau_{\nu,i}} = \prod_i e^{-\Delta\tau_{\nu,i}} = \prod_i \Delta T_{\nu,i} \tag{6}$$

To calculate the Jacobian for the i^{th} grid box,

$$\delta T_\nu = T_\nu(\tau_\nu + \delta\tau_{\nu,i}) - T_\nu(\tau_\nu) = e^{-(\tau_\nu + \delta\tau_{\nu,i})} - e^{-\tau_\nu} \approx -e^{-\tau_\nu} \cdot \delta\tau_{\nu,i} = -T_\nu \cdot \delta\tau_{\nu,i} \tag{7}$$

where $$\delta\tau_{\nu,i} = \frac{2Ar}{\chi} \cdot \frac{\alpha_i \Delta p_i \delta\chi_i}{\alpha_i^2 + (\nu - \nu_0)^2} \tag{8}$$

The Jacobian is defined as

$$J_{\nu,i} = \frac{\delta T_\nu}{(\delta\chi_i / \chi)\cdot(\Delta p_i / P_s)} = -T_\nu \cdot \frac{2r\alpha_i\alpha_s}{\alpha_i^{\,2} + (\nu - \nu_0)^2} \tag{9}$$

Using the finite difference form of T_ν, Eqn. (6)

$$\delta T_\nu = e^{-(\Delta\tau_{\nu,i}+\delta\tau_{\nu,i})} \prod_{j\neq i} e^{-\Delta\tau_{\nu,i}} - \prod_j e^{-\Delta\tau_{\nu,j}} = (e^{-\delta\tau_{\nu,i}} - 1)\prod_j e^{-\Delta\tau_{\nu,j}} \approx -T_\nu \cdot \delta\tau_{\nu,i} \tag{10}$$

The two Jacobians derived from the analytical and finite difference form of the transmittance, Eqns. (10) and (7) are identical.

For cases when the solar zenith angle θ is not zero, $\mu_0 \equiv \cos\theta$ is not equal 1

$$\tau_\nu^{\mu_0} = \frac{r}{\mu_0}\cdot \ln\frac{\alpha_s^2 + (\nu-\nu_0)^2}{(\nu-\nu_0)^2}$$

$$T_\nu^{\mu_0} = e^{-\tau_\nu^{\mu_0}} = \left[\frac{(\nu-\nu_0)^2}{\alpha_s^2 + (\nu-\nu_0)^2}\right]^{r/\mu_0} \tag{11}$$

$$J_{\nu,i}^{\mu_0} = -T_\nu^{\mu_0}\,\frac{1}{\mu_0}\cdot\frac{2r\alpha_i\alpha_s}{\alpha_i^2 + (\nu-\nu_0)^2} \tag{12}$$

2. At the top of the atmosphere

This is similar to the GOSAT/OCO-2 measurements, with μ_0 and μ for incident and reflected zenith angles, and ρ for the surface reflectivity. The transmittance at the top of the atmosphere can be expressed as

$$T_\nu = T_\nu^{\mu_0} \rho T_\nu^{\mu} = \rho \cdot e^{-(\tau_\nu^{\mu_0} + \tau_\nu^{\mu})}$$

$$\delta T_\nu = -T_\nu (\delta\tau_{\nu,i}^{\mu_0} + \delta\tau_{\nu,i}^{\mu})$$

$$T_\nu = \rho \cdot \left[\frac{(\nu - \nu_0)^2}{\alpha_s^2 + (\nu - \nu_0)^2} \right]^{r(1/\mu_0 + 1/\mu)} \tag{13}$$

$$J_{\nu,i} = -T_\nu \left(\frac{1}{\mu_0} + \frac{1}{\mu}\right) \frac{2r\alpha_i\alpha_s}{\alpha_i^2 + (\nu - \nu_0)^2} \tag{14}$$

References

[1] IPCC, Climate Change, the Fourth Assessment *Report* (AR4) of the United Nations Intergovernmental Panel on Climate Change, *Intergovernmental Panel on Climate Change*. 2007.

[2] Yokota, T. *et al.*, Global Concentrations of CO2 and CH4 Retrieved from GOSAT: First Preliminary Results, *Sola*. 2009; **5**, 160-163.

[3] Saitoh, N. *et al.*, CO_2 retrieval algorithm for the thermal infrared spectra of the Greenhouse Gases Observing Satellite: Potential of retrieving CO_2 vertical profile from high-resolution FTS sensor, *Journal of Geophysical Research-Atmospheres*, 2009; **114**, D17305.

[4] Sato, M. *et al.*, FIP's Environmentally Conscious Solutions and GOSAT, *Fujitsu Scientific & Technical Journal*. 2009; **45** (1), 134-140.

[5] Boesch, H. *et al.*, Global characterization of CO_2 column retrievals from shortwave-infrared satellite observations of the Orbiting Carbon Observatory-2 mission, *Remote Sensing*. 2011; **3**(2), 270-304.

[6] Wunch, D., *et al*., Calibration of the Total Carbon Column Observing Network using aircraft profile data, *Atmospheric Measurement Techniques*. 2010;. 3, 2603-2632, doi:10.5194/amtd-3-2603-2010

[7] Wunch D. *et al.*, A method for evaluating bias in global measurements of CO2 total columns from space, *Atmospheric Chemistry and Physics.* 2011; **11**,. 20899-20946 doi:10.5194/acpd-11-20899-2011

[8] Shia, R.-L *et al.*, CO_2 in the upper troposphere: Influence of stratosphere-troposphere exchange, *Geophys. Res. Lett.*, 2006; **33**, L14814, doi:10.1029/2006GL026141.

[9] Jiang, X**.** *et al.*, Simulation of upper troposphere CO2 from chemistry and transport models, *Global Biogeochemical Cycles*, 2008; **22**, GB4025, doi:10.1029/2007GB003049.

[10] Rodgers, C.D., *Inverse Methods for Atmospheric Sounding: Theory and Practice*, Atmospheric, Oceanic and Planetary Physics, Vol. 2. World Scientific, Singapore. 2000.
.

[11] Rothman, L. S. *et. al.*, The HITRAN 2008 molecular spectroscopic database, *J.Q.S.R.T.* 2009; **110**, 533–572. doi:10.1016/j.jqsrt.2009.02.013

[12] Wunch, D. *et al.*, The Total Carbon Column Observing Network (TCCON), *Philos. T. Roy. Soc. A*, 2011; **369**, 2087-2112. doi: 10.1098/rsta.2010.0240

[13] O'Dell, C. W., *et al*: The ACOS CO2 retrieval algorithm Part 1: Description and validation against synthetic observations, Atmos. Meas. Tech., 2012; **5**, 99-121, doi:10.5194/amt-5-99-2012.

[14] Crisp, D., *et al*: The ACOS CO2 retrieval algorithm Part II: Global XCO2 data characterization, Atmos. Meas. Tech., 2012; **5**, 687-707, doi:10.5194/amt-5-687-2012.

[15] Kuai L. *et al.,* Vertically constrained CO_2 retrievals from TCCON measurements, *J.Q.S.R.T.* 2012; **113** (14), 1753-1761, 2012.

[16] Koch, G. J., *et al*., Side-line tunable laser transmitter for differential lidar measurements of CO2: Design and application to atmospheric measurements, *Appl. Opt*. 2008, **47** (7), 944-956.

[17] Tsai, T. R., *et al*. Atmospheric vertical profiles of O3, N2O, CH4, CCl2F2, and H2O retrieved from external-cavity quantum-cascade laser heterodyne radiometer measurements. *Appl. Opt.*, 2012, **51**, (36), 8779-8792.

[18] Trauger, J. T. and J. I. Lunine, Spectroscopy of Molecular Oxygen in the Atmospheres of Venus and Mars, *Icarus*. 1983; **55**, (2), 272-281.